Scaffold based 3-D Cell Culture Imaging Using a Miniature Electrical Impedance Tomography Sensor

Scaffold-based 3-D Cell Culture Imaging Using a Miniature Electrical Impedance Tomography Sensor

Yunjie Yang, *Member, IEEE*, Hancong Wu, Jiabin Jia, *Member, IEEE*, and Pierre O. Bagnaninchi

***Abstract*—3-D Electrical Impedance Tomography (EIT) is an emerging technique for real-time and non-destructive 3-D cell culture imaging. This paper presents a pioneering study of scaffold-based 3-D cell culture imaging using a miniature planar EIT sensor. A 17-electrode miniature-planar EIT sensor equipped with a regular-shape 3-D printed scaffold was manufactured, modelled and characterized. In addition, an efficient 3-D image reconstruction method based on 3-D isotropic Total Variation and *l*1 joint regularization were proposed. Numerical simulation on scaffold phantoms and experimental study on time-varying distribution of MCF-7 cancer cell suspension within the scaffold were performed. Both simulation and experiment results suggest that using the miniature EIT sensor and the developed 3-D image reconstruction algorithms are able to achieve high quality, non-destructive scaffold-based 3-D cell culture imaging.**

***Index Terms*—3-D cell culture; scaffold; Electrical Impedance Tomography (EIT); miniature planar sensor; image reconstruction**

I. Introduction

2-D cell culture has been routinely undertaken in biomedical engineering over decades but is arguably primitive and does not reproduce physiology of a tissue for informative study [1]. By contrast, cell culture using 3-D models has become increasingly prevailing in recent years. Relative to 2-D cell culture, 3-D cell culture demonstrates enhanced cell biological activities which is more biologically relevant to the real complex *in vivo* conditions of living organisms [2]. Among most situations, 3-D cell culture is carried out in a culture dish or bioreactor equipped with scaffolds. Fig. 1 presents the 3-D printed regular-shape scaffold used in this study. Micro porous polymer-based scaffolds can provide mechanical support and a favourable 3-D microenvironment for initial cell attachment and subsequent tissue formation in tissue engineering for tissue replacement, augmentation, tissue support, and drug delivery [3, 4]. However, imaging methodologies to access the *in vitro* cellular activities occurring within the 3-D scaffold construct are limited and most of them are destructive end-point tests, such as histology and Scanning Electron Microscopy (SEM) [5]. Indirect metabolic assays such as MTT assay and presto-blue assay can only provide the lumped value of the cell viability of the entire scaffold [6, 7], while other important parameters such as cell distributions, morphology and characteristics are not discernible. The existence of scaffold raises a tough challenge for 3-D cell culture imaging attributing to the spatial constraints imposed by the scaffold structure on the change of biological properties. As a result, real-time and non-destructive sensing technique with favourable temporal-spatial resolution is desperately desirable for the study of biological behaviour and to perform long-term monitoring of fast cellular activities, such as cell-drug interaction, bone tissue regeneration, etc. However, to date few techniques possessing such capabilities have been comprehensively investigated and maturely applied.

In this work, we demonstrate a pioneering study of scaffold-based 3-D cell culture imaging using a miniature-planar Electrical Impedance Tomography (EIT) sensor. EIT is an electrical field based tomographic modality which performs the recovery of the conductivity within interior of a domain based on boundary-applied currents and induced voltage measurements [8-11]. EIT has been investigated extensively in biomedical imaging [11, 12] and industrial process imaging [11, 13] with many successful cases. Preliminary efforts in applying EIT in imaging 3-D cell culture by the authors have been reported earlier [14-16]. In this occasion, as the follow-up work, the feasibility of performing efficient scaffold-based 3-D cell culture imaging is thoroughly investigated. A miniature EIT sensor equipped with a 3-D printed regular-shape scaffold was described, modelled and characterized. In addition, a 3-D image reconstruction method based on 3-D isotropic Total Variation and l_1 joint regularization was proposed to generate high quality conductivity images offline in a 3-D format. Numerical simulation on scaffold phantoms and experimental study on MCF-7 human breast cancer cell distribution inside the scaffold were carried out to verify the feasibility of this idea.

The paper is organized as follows. Section II provides the fundamental theory of EIT. Section III presents the design, manufacture and characterization of the miniature EIT sensor and demonstrates 3-D image reconstruction algorithms. Section IV gives simulation and experimental results. Finally, Section V draws conclusions and briefly discusses the future work.

Manuscript received XXX.

The research was supported by XXX.

Y. Yang, H. Wu and J. Jia, are with the Agile Tomography Group, Institute for Digital Communications, School of Engineering, The University of Edinburgh, Edinburgh, UK. (e-mail: y.yang@ed.ac.uk).

P. Bagnaninchi is with the MRC Centre for Regenerative Medicine, The University of Edinburgh, Edinburgh, UK.

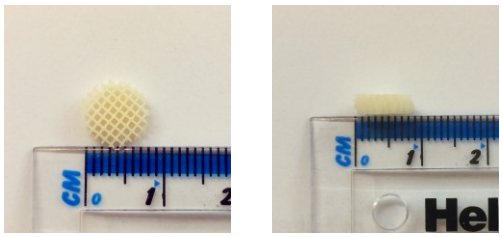

(a) (b)

Fig. 1. Picture of a regular-shape scaffold (a) top view and (b) side view.

II. Electrical Impedance Tomography

Fig. 2 illustrates the sensing principle of EIT. Given the sensing region $\Omega \subset \mathbb{R}^q$ where $q = 2, 3$, in EIT, a set of electrodes is attached to the boundary of the sensing region $\partial\Omega$. Complimentary currents are injected sequentially to the sensing region through selected electrode pairs and induced boundary potentials are measured. Utilizing the measurements, conductivity within the sensing region is estimated by solving a typical inverse problem [8]. In condition of certain assumptions, the measurements can be modelled by the Complete Electrode Model (CEM) [17, 18], which is given by:

$$\nabla \cdot \big(\sigma(x,y)\nabla u(x,y)\big) = 0, \ \ (x,y) \in \Omega \tag{1}$$

$$u + z_\ell \sigma \frac{\partial u}{\partial n} = U_\ell, \ (x,y) \in e_\ell, \ \ell = 1, \dots, \mathcal{L} \tag{2}$$

$$\int_{e_\ell} \sigma \frac{\partial u}{\partial n} dS = I_\ell, \ \ell = 1, \dots, \mathcal{L} \tag{3}$$

$$\sigma \frac{\partial u}{\partial n} = 0, \ (x,y) \in \partial\Omega \setminus \cup_{\ell=1}^{\mathcal{L}} e_\ell \tag{4}$$

where σ and u denote respectively the conductivity and electric potential inside Ω; $\mathcal{L}$ is the number of electrodes and e_ℓ is the ℓ^{th} electrode; z_ℓ represents the contact impedance of e_ℓ; n is the outward unit norm of the boundary $\partial\Omega$; U_ℓ and I_ℓ represent the electrical potential and injected current on e_ℓ, respectively.

Additionally, the following conditions should be met in order to guarantee the existence and uniqueness of the solution u.

$$\sum_{\ell=1}^{\mathcal{L}} I_\ell = 0, \ \sum_{\ell=1}^{\mathcal{L}} U_\ell = 0. \tag{5}$$

The CEM describes a nonlinear relation between the conductivity in Ω and the current-induced boundary measurements. Taking into account the requirement of real-time imaging performance in 3-D cell culture monitoring, the linearized EIT model is adopted in this work, as expressed by:

$$\Delta V = J\Delta\sigma \tag{6}$$

where $\Delta V \in \mathbb{R}^m$ is the voltage change due to a conductivity perturbation $\Delta\sigma \in \mathbb{R}^n$ with respect to a reference $\sigma_0 \in \mathbb{R}^n$. $J \in$

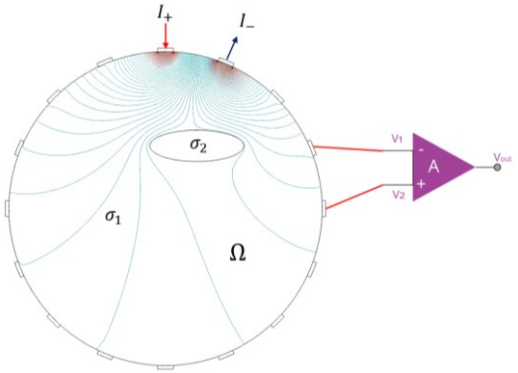

Fig. 2. Sensing principle of EIT.

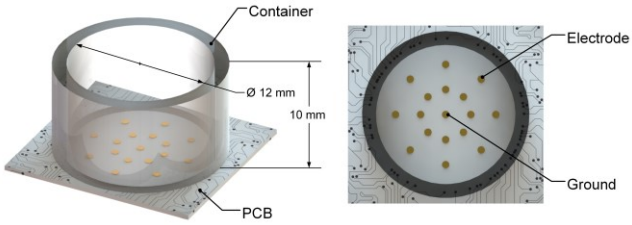

Fig. 3. Schematic illustration of the miniature EIT sensor.

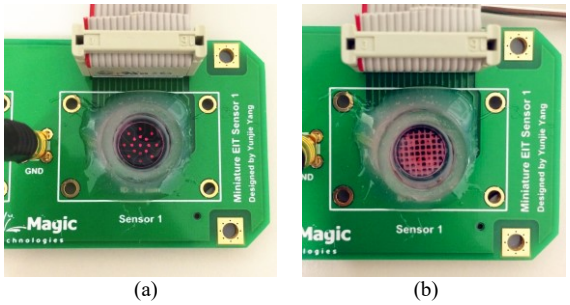

(a) (b)

Fig. 4. Picture of (a) the manufactured miniature EIT sensor and (b) the sensor equipped with a regular-shape scaffold.

$\mathbb{R}^{m\times n}$ denotes the Jacobian matrix, where m is the number of measurements and n is the number of pixels/voxels, and it can be calculated by [19]:

$$J_{i,j,k} = -\int_{voxel\ k} \nabla u_i \cdot \nabla u_j \, dV \tag{7}$$

where $J_{i,j,k}$ is the sensitivity at voxel (i,j,k). u_i and u_j represent electrical potential distribution when the i^{th} and j^{th} electrode pairs are injected with currents, respectively.

Estimate of conductivity is based on standard least square methods [20], which in general can be formulated as the following format:

$$\Delta\sigma_{est} = \arg\min_{\Delta\sigma}\{\|\Delta V - J\Delta\sigma\|^2 + \beta\mathcal{M}(\Delta\sigma)\} \tag{8}$$

where $\Delta\sigma_{est} \in \mathbb{R}^n$ denotes the estimate of conductivity. $\beta \in \mathbb{R}$ is regularization parameter. $\mathcal{M}(\Delta\sigma)$ represents the regularization term.

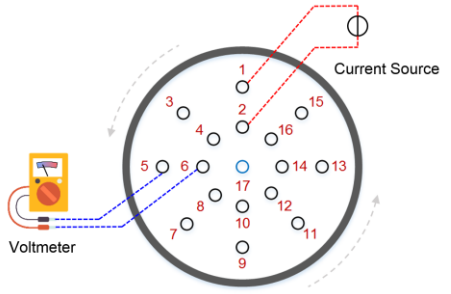

Fig. 5. Electrode numbering and adjacent sensing stategy.

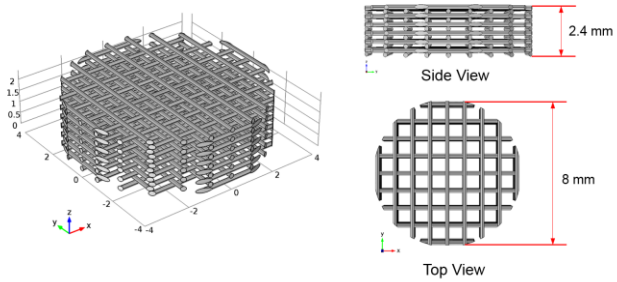

Fig. 6. Modelling of the regular shape scaffold.

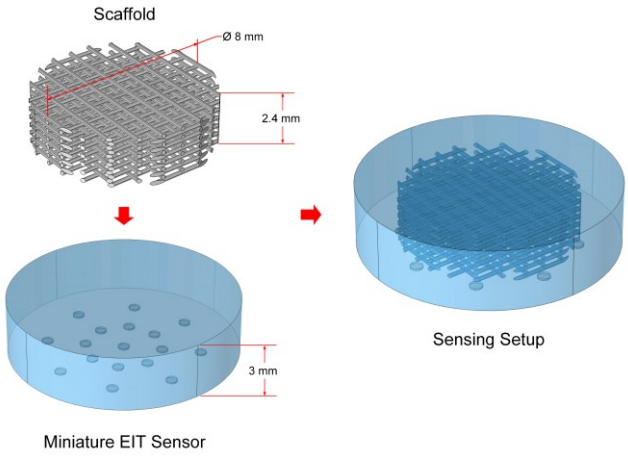

Fig. 7. Modelling of the miniature EIT sensor equipped with the scaffold.

III. Sensor and Image Reconstruction

A. Miniature EIT Sensor

A 17-electrode miniature EIT sensor recently designed by the authors [21] were employed in this work to study scaffold-based 3-D cell culture imaging. Fig. 3 presents the schematic presentation of the sensor. A transparent cylindrical chamber (inner diameter: 12 mm; height: 10 mm) was assembled on a Printed Circuit Board (PCB) substrate. There are 17 gilded circular electrodes (diameter: 0.3 mm) evenly distributed on the substrate. The sensing electrodes are located along two concentric circles with 8 electrodes evenly distributed on each circle. In addition, an extra electrode is located at the center acting as a reference point. These radically distributed planar electrodes could generate a 3-D sensitive region along the vertical direction near the substrate [22]. This characteristic was utilized to perform 3-D near-surface conductivity imaging. Fig. 4 (a) presents the picture of the manufactured sensor filled with cell culture medium and Fig. 4 (b) shows the sensor equipped with a regular-shape scaffold.

Fig. 5 shows the electrode numbering from top view and the schematic illustration of adjacent sensing strategy [23] employed in this work, i.e. selecting electrode {1, 2} as current injection, electrode {3, 4}, {4, 5}, …, {15, 16} as differential voltage measurements, then subsequently changing current injection electrodes until all the measurements are taken. A complete scan of this sensing strategy consists of 104 independent measurements, from which conductivity distribution can be estimated based on Eq. (8).

B. Scaffold Modelling and Analysis

To numerically investigate the feasibility of imaging 3-D cell culture by the presented sensor equipped with a regular shape scaffold, as well as the effect of scaffold on 3-D imaging quality, a 3-D geometric model of the regular shape scaffold was established in COMSOL Multiphysics. Fig. 6 illustrates the modelling of the regular shape scaffold. The diameter and height of the scaffold are 8 mm and 2.4 mm, respectively, which are in consistent with the actual scaffold used in the experimental study. The conductivity of the scaffold material is 0.001 mS/cm.

Fig. 7 shows the modelling of miniature EIT sensor equipped with the scaffold. Saline was selected as homogeneous background medium in this model. Its conductivity was set to be 20 mS/cm, which was similar with the cell culture medium used in this work. The height of effective sensing region was set to be 3 mm. The amplitude of injected currents was 1 mA.

Regarding this sensing setup, one of the most interesting aspects is the variation of spatial current density distribution after the presence of the scaffold. Fig. 8 (a) and Fig. 8 (b) present comparison of logarithmic current density norm on the vertical cross section in the center (as indicated by the red plane in the figure), where electrode 1 and 2 were injected with a pair of complementary currents. Note that in these two figures, different colorbars were applied, which may result in different representations for the same current density. Fig. 8 (c) illustrates the logarithmic current density norm along a transverse line z=1.5 at the vertical cross section. Simulation results shown in Fig. 8 suggest that the injected current can penetrate the scaffold cavities and current density amplitudes are similar at the scaffold cavities for the two cases with and without the scaffold, in addition to the fact that current density approaches zero at the locations of the scaffold structure. The results suggested the feasibility of performing 3-D conductivity imaging within the cavities of the scaffold.

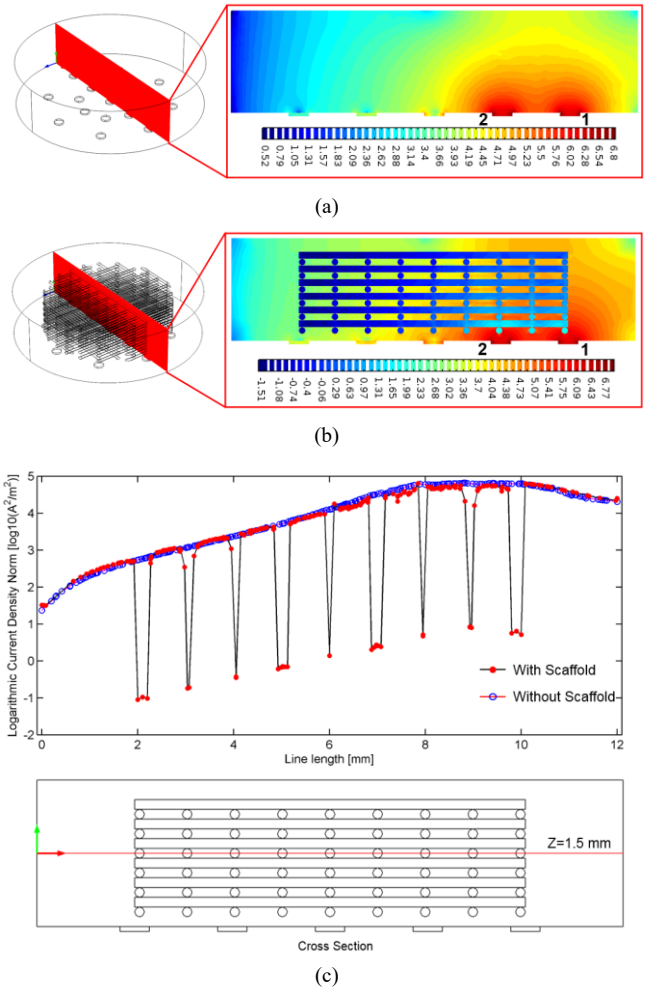

Fig. 8. Comparison of logarithmic current density of (a) sensor without scaffold and (b) sensor with scaffold and (c) at the transverse line z=1.5.

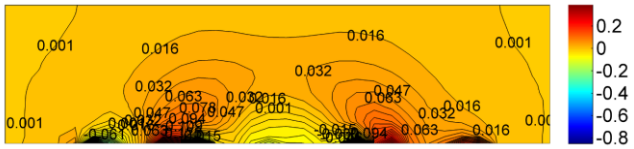

Fig. 9. Contour plot of sensitivity distribution on the vertical cross section shown in Fig. 8 (a).

Fig. 9 shows the contour plot of spatial sensitivity distribution on the vertical cross section indicated in Fig. 8 (a) (the red plane). The sensitivity region has a trapezoidal shape along the vertical direction, which indicates the possibility of detecting objects within the 3-D domain. Further validation of 3-D imaging capability are demonstrated in Section 4 of this paper through simulation studies and experiments.

C. 3-D Image Reconstruction Method

A specific type of 3-D conductivity variation is considered in this work, i.e. the conductivity variation induced by the cells inside the scaffold cavities. 3-D conductivity is estimated by using a Finite Element Method (FEM) implementation of the forward model. Fig. 10 (a) shows the fine mesh for forward problem calculation and Fig. 10 (b) presents the coarse mesh for inverse problem calculation. The fine mesh consists of

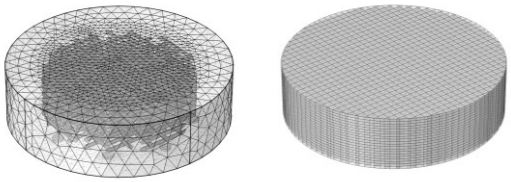

(a) (b)

Fig. 10. FEM Mesh for (a) forward problem and (b) inverse problem calculation.

741,569 domain elements. The inverse mesh is composed of 16240 cuboid elements with 20 vertical layers and 812 elements on each layer.

Considering the size of the scaffold, its induced conductivity variation is spatially distributed in a large scale. In contrast, the conductivity variation, which happens in the cavities of the scaffold, can be spatially distributed in a much smaller scale and the amplitude is typically weak and piece-wise continuous. This case is of more interest in practice and especially critical in a practical 3-D cell culture process. In order to obtain better image qualities based on weak measurement signal and promote sparse solutions with explicit boundaries, a 3-D image reconstruction algorithm is proposed based on 3-D isotropic Total Variation (TV) and l_1 joint regularization (3-D-TV-l_1), which is formulated as:

$$\Delta\sigma_{est} = \arg\min_{\Delta\sigma}\{\|\Delta V - J\Delta\sigma\|^2 + \lambda_1 \mathrm{TV}_{3\mathrm{D}}(\Delta\sigma) + \lambda_2\|\Delta\sigma\|_1\} \quad (9)$$

where $\lambda_i \in \mathbb{R}, i = 1,2$ denotes the regularization parameters. Note that in this context, ΔV refers to the voltage change with respect to the configuration with scaffold, and J refers to homogenous saline solution equipped with scaffold. The 3-D TV of conductivity, i.e. $\mathrm{TV}_{3\mathrm{D}}(\Delta\sigma)$, is defined as:

$$\mathrm{TV}_{3\mathrm{D}}(\Delta\sigma) = \sum_x \sum_y \sum_z D_{x,y,z} \quad (10)$$

where $(x, y, z) \in \Omega$, $D_{x,y,z}$ denotes the discrete variation transform as defined by:

$$D_{x,y,z} = \left|\Delta\sigma_{x,y,z} - \Delta\sigma_{x+1,y,z}\right| + \left|\Delta\sigma_{x,y,z} - \Delta\sigma_{x,y+1,z}\right| + \left|\Delta\sigma_{x,y,z} - \Delta\sigma_{x,y,z+1}\right| \quad (11)$$

Equation (9) is non-differentiable at origin point. Whilst by introducing the approximation of TV's gradient [14] and the sub-gradient of l_1 norm [24], gradient-based approaches such as Newton's method can be applied to trace a local minimum of Eq. (9). Accordingly, the iteration form of solving Eq. (9) can be formulated as:

$$\Delta\sigma_{x,y,z}^{i+1} = \Delta\sigma_{x,y,z}^{i} - \mathfrak{Z}^i\left\{\nabla_{x,y,z}\mathcal{F}_{\lambda_1}(\Delta\sigma^i) + \lambda_2\nabla_{x,y,z}\left(\left\|\Delta\sigma^i\right\|_1\right)\right\} \quad (12)$$

where $\mathfrak{Z}^i$ denotes the step size of the i^{th} iteration, which is calculated based on the backtracking line search technique with

the initial step size $\lambda^0 = 0.5$, which implementation details can be found in [25]. In addition, we have

$$\nabla_{x,y,z}\mathcal{F}_{\lambda_1}(\Delta\sigma^i) = \{J^{\mathrm{T}}(J\Delta\sigma^i - \Delta V)\}_{x,y,z} + \cdots \lambda_1\nabla_{x,y,z}\left(\mathrm{TV}_{3\mathrm{D}}(\Delta\sigma^i)\right) \quad (13)$$

where the gradient of TV, i.e. $\nabla_{x,y}\left(\mathrm{TV}(\Delta\sigma^i)\right)$, can be calculated approximately by using proper relaxation. The detail regarding this part can be referred to our previous work [14].

The sub-gradient of l_1 norm $\nabla_{x,y}\left(\|\Delta\sigma^i\|_1\right)$ is defined as:

$$\nabla_{x,y,z}\left(\|\Delta\sigma^i\|_1\right) = \begin{cases} sign(\Delta\sigma^i_{x,y,z}), & |\Delta\sigma^i_{x,y,z}| \geq \mu \\ 1, & |\Delta\sigma^i_{x,y,z}| < \mu,\ \nabla_{x,y,z}\mathcal{F}_{\lambda_1}(\Delta\sigma^i) < -\lambda_2 \\ -1, & |\Delta\sigma^i_{x,y,z}| < \mu,\ \nabla_{x,y,z}\mathcal{F}_{\lambda_1}(\Delta\sigma^i) > \lambda_2 \\ 0, & |\Delta\sigma^i_{x,y,z}| < \mu,\ |\nabla_{x,y,z}\mathcal{F}_{\lambda_1}(\Delta\sigma^i)| \leq \lambda_2 \end{cases} \quad (14)$$

where μ is a positive relaxation factor which is selected as 1e-7 in this work in order to define a small enough interval containing the origin where the l_1 norm is non-differentiable.

The implementation of 3-D-TV-l_1 is summarized in **Algorithm 1**. In this work, correlation coefficient is employed to evaluate quantitatively the accuracy of the reconstruction results for the conductivity within the scaffold cavities. The correlation coefficient is defined by:

$$C_{corr} = \frac{\sum_{i=1}^{n}(\widehat{\Delta\sigma}_i - \overline{\widehat{\Delta\sigma}})(\Delta\sigma_i - \overline{\Delta\sigma})}{\sqrt{\sum_{i=1}^{n}(\widehat{\Delta\sigma}_i - \overline{\widehat{\Delta\sigma}})^2 \sum_{i=1}^{n}(\Delta\sigma_i - \overline{\Delta\sigma})^2}} \quad (15)$$

where $\Delta\sigma_i$ and $\widehat{\Delta\sigma}_i, i = 1, \ldots, n$ denote respectively the i^{th} element of the true conductivity and estimated conductivity. $\overline{\widehat{\Delta\sigma}}$ and $\overline{\Delta\sigma}, i = 1, \ldots, n$ denote respectively the mean of the estimated conductivity and true conductivity. Correlation coefficient evaluates the degree to which the distribution of the estimated conductivity and ground truth are associated. A larger value indicates a better result.

Algorithm 1
3-D Total Variation and l_1 joint regularization (3-D-TV-l_1)

Input: Voltage ΔV, regularization parameters λ_1 and λ_2, maximum iteration k.

Initialization: Set $\Delta\sigma_0 = Q$, where $Q \in \mathbb{R}^n$ is an all zero vector.

For $l = 1, 2, \ldots, k$

(1): Update the gradient $\nabla_{x,y}\left(\mathrm{TV}(\Delta\sigma^i)\right)$.

(2): Update $\nabla_{x,y,z}\mathcal{F}_{\lambda_1}(\Delta\sigma^i)$ based on Eq. (13).

(3): Update sub-gradient $\nabla_{x,y}\left(\|\Delta\sigma^i\|_1\right)$ using Eq. (14).

(4): Update $\Delta\sigma^{i+1}_{x,y,z}$ using Eq. (12).

(5): $l \leftarrow l + 1$.

End For

Output: The estimated conductivity $\Delta\sigma_{est}$.

IV. Result and Discussion

A. Numerical Simulation Results

Experiments based on simulated phantoms were conducted first to examine the feasibility of imaging scaffold-based 3-D cell culture by using the presented sensor. As mentioned previously, conductivity change within the cavities of the scaffold is of particular interest. In this part, three simulated phantoms were established to study the 3-D imaging performance regarding this type, i.e. two small spheroid phantoms with different vertical locations as shown in Fig. 11 (a) and (b) and the cylinder phantom as shown in Fig. 11 (c). The diameter of the spheroids and cylinders is 0.3 mm and the height of cylinders is 2.4 mm. The small spheroid phantoms simulate a cell spheroid and the cylinder phantom simulates a cavity filled with cells. The conductivity of the spheroids and cylinders is 1e-4 mS/cm and 40 mS/cm, respectively. The background substance is saline; the conductivity is 20 mS/cm. For all phantoms, the simulated data were added with Gaussian noise and the Signal to Noise Ratio (SNR) was 50 dB.

In practical cases of cell imaging, we only focus on conductivity changes within the cavities of the scaffold since imaging of the static scaffold is unnecessary. In order to image the conductivity changes happening in scaffold cavities, a reference measured on homogenous saline equipped with an empty scaffold was employed in the 3-D image reconstruction procedures. For these cases, **Algorithm 1** was applied for 3-D image reconstruction in order to obtain a sparse estimate. When **Algorithm 1** was implemented, the maximum iteration number was set as 150 and the elapsed time was 1.6747s on a PC with MATLAB 2017b, 24GB RAM memory and an Intel Xeon X5650 CPU. The regularization parameters λ_1 and λ_2 were set as 0.001 and 0.0001, respectively, based on a series of practice.

Fig. 12 presents the 3-D image reconstruction results. The sliced images show the horizontal cross sections from the bottom (layer 1) to the top (layer 20) of the sensing domain. The 3-D synthesized image illustrates the isosurface of a

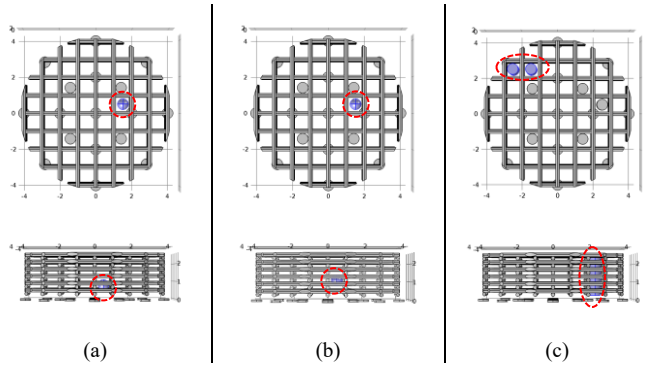

Fig. 11. Simulation phantoms. (a) Phantom 1: a small speriod (z=0.8mm). (b) Phantom 2: a small speriod (z=1.1mm) (c) Phantom 3: two cylinders.

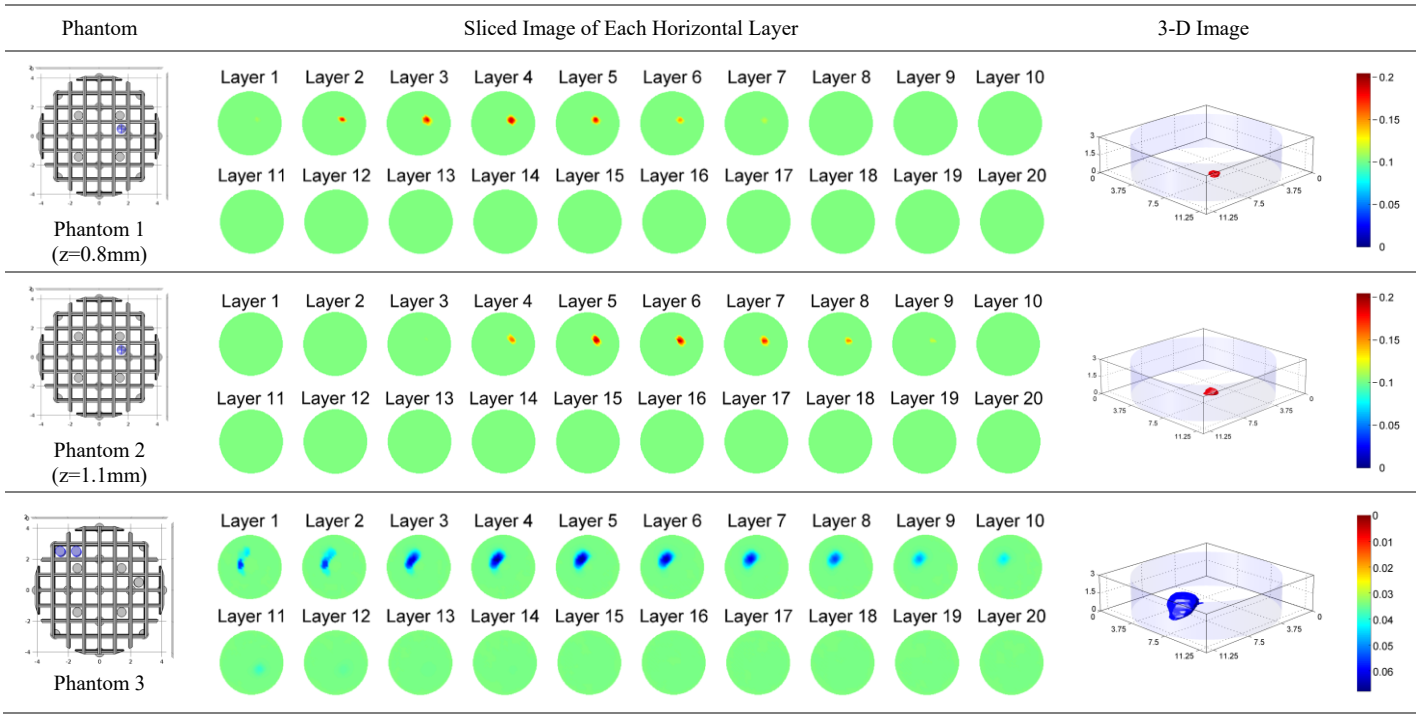

Fig. 12. 3-D image reconstructions of simulation phantoms.

quarter of the maximum conductivity change value.

The first and second rows of Fig. 12 show the imaging results of spheroid phantoms with different vertical locations. In this occasion, the small-scale conductivity changes were well captured with superior noise reduction performance. The locations of the two spheroids were correctly estimated. The correlation coefficients of the phantoms are 0.6825 and 0.6641, respectively.

The fourth row of Fig. 12 presents 3-D image reconstruction result of two cylinders phantom. Conductivity change happening within two scaffold cavities can also be explicitly estimated. Correlation coefficient of this phantom is 0.5963. Comparing the results, relatively better image quality was obtained by the spheroid phantoms, which can be attributed to the following reasons: a) characteristics of sensitivity; since planar electrode configuration is employed due to geometrical limitation, sensitivity is relatively week near the top area of the sensing region (see Fig. 9), which may introduce error in reconstructing conductivity near that area; b) model error; as the spheroid phantoms contribute smaller conductivity change, they suffer smaller linearization error compared to the cylinder phantom.

Judging from the results, we can expect that the proposed miniature EIT sensor and 3-D image reconstruction method are able to estimate the conductivity change occurred within the cavities of the scaffold in 3-D cell culture processes.

B. Experiment Results

Cellular imaging experiments using real-time measurement data were conducted to verify the feasibility of applying the proposed methods in estimating dynamic cellular distribution within the scaffold. The scaffold used in the experiment was printed using Ultimaker 2 3-D Printer (Ultimaker, UK) by Fused Deposition Modelling (FDM) using Poly Lactic Acid (PLA). The 3-D printed regular-shape scaffold was placed in the Dulbecco's Modified Eagle Medium (DMEM) based culture medium, which conductivity is 20 mS/cm. A small volume of cell suspension, i.e. 0.02 ml, was delivered to a specific scaffold cavity by using a sterilized syringe. Since the conductivity of cell suspension is lower than the cell culture medium, a local conductivity contrast would emerge and gradually change due to the diffusion within the scaffold. This is well-suited to verify the dynamic imaging performance, and to explore the viability to image cell proliferation within the scaffold.

Fig. 13 shows the cell suspension to be imaged. In preparation of the suspension, the MCF-7 breast cancer cells were obtained from ATCC (Middlesex, UK) and were first cultured in the T-25 flask in the DMEM based culture medium composed of 89% DMEM with glutamax, 10% Fetal Bovine Serum (FBS) and 1% penicillin/streptomycin for more than 5 passages, which can remove DMSO and dead cells that might affect your seeding density calculation. They were then recovered by using 0.25% Trypsin and suspended into 5ml culture medium. The size of the cells in the suspension was around 20 microns. In order to increase the cell concentration, centrifugation was applied to harvest the cell pellet and to suspend them into 0.25ml culture medium to obtain a cell suspension with a 5.06×107 cells/ml concentration. Because of the presence of the insulating double-lipid bilayer membrane, the cells were less conductive than the culture medium at low frequencies. Therefore, the conductivity of the cell suspension was lower than that of the culture medium.

The 3-D multi-frequency biomedical EIT system developed by the authors at the Agile Tomography Group, University of Edinburgh [26], was employed to acquire real-time impedance measurements in this study. The system has 32 electrode interfaces and its excitation current's frequency ranges from 10 kHz up to 1 MHz. The system presents the combination of several advantageous features such as fully adjustable multi-frequency current source, flexible switching scheme, high SNR (82.82 dB on a normal size 2-D sensor) and high-speed data acquisition (up to 1014 frames per second) [26]. In addition, a 3-D imaging software named *Visual Tomography* was also built for real-time 2-D and 3-D image reconstruction, data analysis and visualization. In this work, a fixed current frequency of 10 kHz was applied through all the experiments. Under the experimental setting, the SNR was measured to be 52.80 dB on the miniature sensor.

Algorithm 1 was utilized to estimate the time-varying conductivity change based on real-time voltage measurements. The maximum iteration number was set to be 400 (elapsed time is 3.5974s under the same computer configuration) and the regularization parameters λ_1 and λ_2 were set as 0.1 and 0.005, respectively, based on a series of practice.

Fig. 14 shows the measured voltage response near the point of cell suspension delivery, i.e. the 71th measurement. Before time point 3.33s, the cell suspension was not delivered and the voltage response was relatively steady. At time point 3.33s, 0.02 ml cell suspension was released into the scaffold and the increase of the measured voltage could be observed. After time point 4.54s, the voltage measurement tends to be stable again which indicates a steady state of the mixture was reached. The measurement obtained at time point 0.33s was adopted as a reference, and 3-D images at six time points as indicated in Fig. 15 with a red circle were reconstructed. The results are presented in Fig. 15.

From the 3-D image reconstructions based on the time series measurement, we can see that at time point 3.03s, there is no conductivity variation emerged. From time point 3.63s to time point 4.24s, a gradually increasing conductivity area near the cell suspension delivery point can be observed explicitly. While from time point 4.54s to 6.66s, the conductivity variation area remains comparable but slightly decreases with time in terms of area and amplitude. The changing trend of conductivity, which is observed from the 3-D reconstructions, accords well with the time-varying voltage response as illustrated in Fig. 15. The results suggest that the conductivity contrast induced by less conductive cell suspension within the scaffold cavities can be well reconstructed by using the sensor demonstrated and the algorithm proposed. This verified the viability to image cell proliferation within the scaffold in a practical cell culture environment.

C. Discussions

Several critical aspects in this study, such as the impact of model error and selection of regularization parameters, are discussed in this subsection.

a) Model errors. The linearized EIT model as depicted by Eq. (6) was utilized in this study to fulfil the requirement of efficient 3-D imaging. Since the multi-frequency EIT system could operate at a frame rate up to 1014 fps, low computation cost and complexity in the data/image analysis procedure is more preferable and practical.

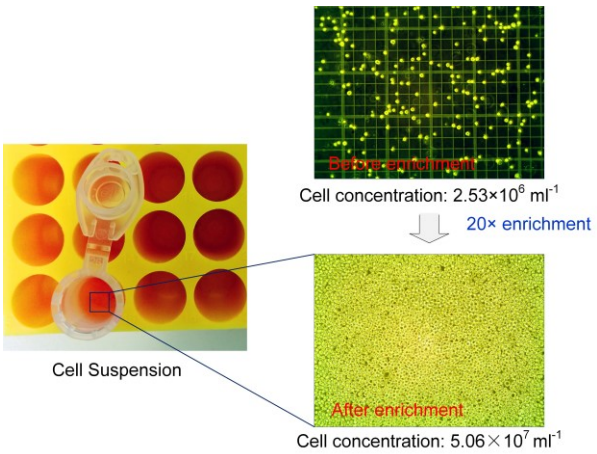

Fig. 13. The cell suspension to be imaged.

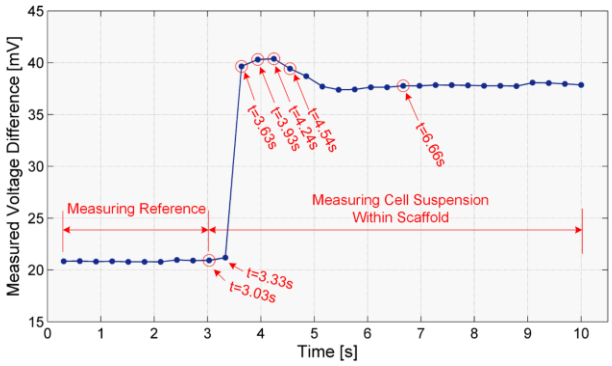

Fig. 14. Measured voltage response near the point of cell suspension delivery.

The EIT-image-reconstruction problem in essence is non-linear. Utilization of linearized model can introduce model errors especially for the cases with relatively large conductivity perturbation and fine details. Evaluation of model error introduced by the linearization process has been thoroughly studied in several work published previously [23, 27, 28]. In this study, although the conductivity variation induced by scaffold is large in scale, for scaffold-based 3-D cell culture imaging, we mainly focus on conductivity changes within the cavities of the scaffold, as imaging of the static scaffold itself is unnecessary. Due to the structural constraint of the scaffold, the conductivity changes happening within the scaffold interspace are generally small in dimension and weak in amplitude, and preferable image quality can be obtained by using the linearized EIT model.

b) Regularization parameters. Proper selection of regularization parameters is critical in solving inverse problems using regularization techniques. In the past, significant effort has been made in investigating systematic rules in selecting appropriate regularization parameters, such as the L-curve method [29], which is one of the simplest and most popular

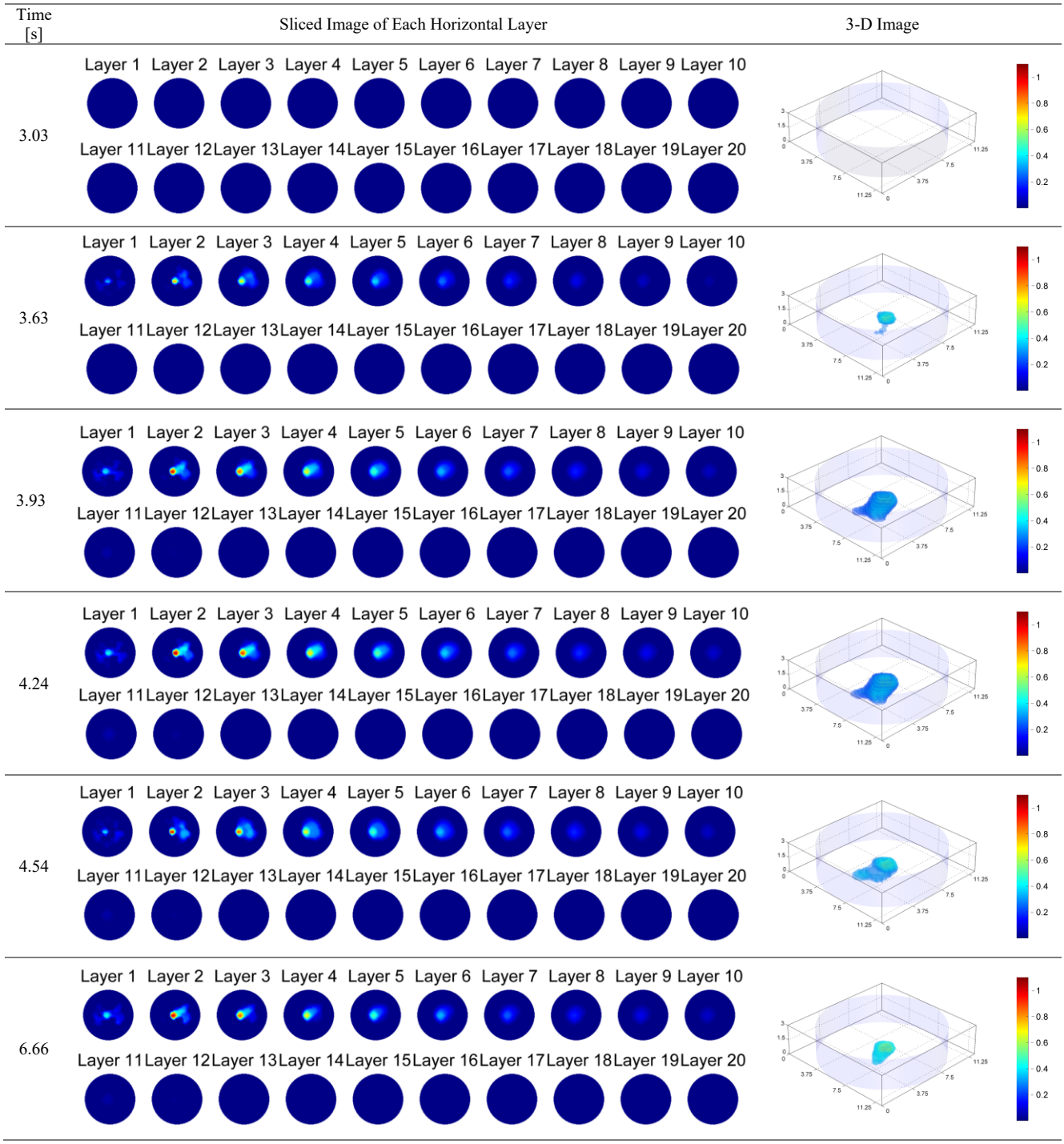

Fig. 15. 3-D image reconstructions using real-time experiment data.

methods for selecting a single regularization parameter when no other noise properties are known. For such methods, regularization term are usually required to be continuously differentiable and convex.

In this study, we proposed an image reconstruction method by combining two non-smooth penalty functions, i.e. l_1 and 3-D TV, in order to produce models with multiple desired characteristics. In this case, however, conventional parameter selection methods are difficult to be applied directly, because both regularization terms here are not continuously differentiable. In addition, for this multiple- constrained regularization approach, a multi-parameter generalization of the conventional method is also required [30]. For these reasons, regularization parameters in this work were selected based on a series of practice, i.e. the combination of a set of parameters [1000, 100, 10, 1, 0.1, 0.05, 0.01, 0.005, 0.001, 0.0001] are gradually tuned to obtain the best results.

In the future, more efforts will be made to investigate optimal parameter section method for multiple-constrained regularization with non-smooth penalty functions as a separate study, based on the state-of-the-art research outcomes, such as the most recently reported work in [31].

V. Conclusion

This paper proposed a non-destructive imaging technique for scaffold-based 3-D cell culture systems by utilizing a miniature EIT sensor. The major contribution of this work includes:

- The feasibility of performing 3-D conductivity imaging within scaffold cavities was theoretically validated by FEM.
- A 3-D-TV and l_1 joint regularization algorithm was developed to realize accurate estimation of small-scale conductivity distributions.
- 3-D dynamic cell distribution imaging experiments demonstrated that by using the miniature EIT sensor and the developed algorithm, conductivity variation induced by MCF-7 cancer cell suspension within the cavities of the scaffold could be captured accurately in a real-time, non-destructive and 3-D manner.
- The outcomes provides a promising method for online visualization and characterization of multicellular aggregate within scaffold-based 3-D cell culture systems.

In future work, long-term scaffold-based 3-D cell culture processes imaging in a practical cell culture environments, such as the imaging of cell proliferation and bone formation, will be studied. The feasibility of imaging different cell distributions at multiple locations will also be investigated.

References

[1] M. Ravi, V. Paramesh, S. R. Kaviya, E. Anuradha, and F. D. P. Solomon, "3D Cell Culture Systems: Advantages and Applications," (in English), *Journal of Cellular Physiology,* vol. 230, no. 1, pp. 16-26, Jan 2015.

[2] E. Cukierman, R. Pankov, D. R. Stevens, and K. M. Yamada, "Taking cell-matrix adhesions to the third dimension," (in English), *Science,* vol. 294, no. 5547, pp. 1708-1712, Nov 23 2001.

[3] D. W. Hutmacher, "Scaffold design and fabrication technologies for engineering tissues—state of the art and future perspectives," *Journal of Biomaterials Science, Polymer Edition,* vol. 12, no. 1, pp. 107-124, 2001.

[4] M. Martina and D. W. Hutmacher, "Biodegradable polymers applied in tissue engineering research: a review," *Polymer International,* vol. 56, no. 2, pp. 145-157, 2007.

[5] L. E. Smith, R. Smallwood, and S. Macneil, "A comparison of imaging methodologies for 3D tissue engineering," *Microscopy research and technique,* vol. 73, no. 12, pp. 1123-1133, 2010.

[6] T. R. Olsen *et al.*, "Manipulation of cellular spheroid composition and the effects on vascular tissue fusion," *Acta Biomaterialia,* vol. 13, no. Supplement C, pp. 188-198, 2015/02/01/ 2015.

[7] C. Holmes, J. Daoud, P. O. Bagnaninchi, and M. Tabrizian, "Polyelectrolyte Multilayer Coating of 3D Scaffolds Enhances Tissue Growth and Gene Delivery: Non‐Invasive and Label‐Free Assessment," *Advanced healthcare materials,* vol. 3, no. 4, pp. 572-580, 2014.

[8] R. H. Bayford, "Bioimpedance tomography (Electrical impedance tomography)," (in English), *Annual Review of Biomedical Engineering,* vol. 8, pp. 63-91, 2006.

[9] S. Liu, J. Jia, Y. D. Zhang, and Y. Yang, "Image Reconstruction in Electrical Impedance Tomography Based on Structure-Aware Sparse Bayesian Learning," *IEEE Transactions on Medical Imaging,* 2018.

[10] J. Yao, H. Obara, A. Sapkota, and M. Takei, "Development of three-dimensional integrated microchannel-electrode system to understand the particles' movement with electrokinetics," (in English), *Biomicrofluidics,* vol. 10, no. 2, Mar 2016.

[11] J. F. Yao and M. Takei, "Application of Process Tomography to Multiphase Flow Measurement in Industrial and Biomedical Fields: A Review," (in English), *IEEE Sensors Journal,* vol. 17, no. 24, pp. 8196-8205, Dec 15 2017.

[12] A. Meir and B. Rubinsky, "Electrical impedance tomographic imaging of a single cell electroporation," (in English), *Biomedical Microdevices,* vol. 16, no. 3, pp. 427-437, Jun 2014.

[13] T. Wondrak and M. Soleimani, "A novel metal flow imaging using electrical capacitance tomography," (in English), *Measurement Science and Technology,* vol. 28, no. 6, Jun 2017.

[14] Y. J. Yang, J. B. Jia, S. Smith, N. Jamil, W. Gamal, and P. O. Bagnaninchi, "A Miniature Electrical Impedance Tomography Sensor and 3-D Image Reconstruction for Cell Imaging," (in English), *IEEE Sensors Journal,* vol. 17, no. 2, pp. 514-523, Jan 15 2017.

[15] X. Yin, Y. Yang, J. Jia, and C. Tan, "3D image reconstruction on a miniature planar EIT sensor using sparsity with median filter," in *2017 IEEE SENSORS*, 2017, pp. 1-3.

[16] Y. Yang, "Advanced digital electrical impedance tomography system for biomedical imaging," 2018.

[17] K. S. Cheng, D. Isaacson, J. C. Newell, and D. G. Gisser, "Electrode Models for Electric-Current Computed-Tomography," (in English), *IEEE Transactions on Biomedical Engineering,* vol. 36, no. 9, pp. 918-924, Sep 1989.

[18] E. Somersalo, M. Cheney, and D. Isaacson, "Existence and Uniqueness for Electrode Models for Electric-Current Computed-Tomography," (in English), *Siam Journal on Applied Mathematics,* vol. 52, no. 4, pp. 1023-1040, Aug 1992.

[19] N. Polydorides and W. R. B. Lionheart, "A Matlab toolkit for three-dimensional electrical impedance tomography: a contribution to the Electrical Impedance and Diffuse Optical Reconstruction Software project," (in English), *Measurement Science and Technology,* vol. 13, no. 12, pp. 1871-1883, Dec 2002.

[20] W. Q. Yang and L. H. Peng, "Image reconstruction algorithms for electrical capacitance tomography," (in English), *Measurement Science and Technology,* vol. 14, no. 1, pp. R1-R13, Jan 2003.

[21] X. Yin, H. Wu, J. Jia, and Y. Yang, "A Micro EIT Sensor for Real-time and Non-destructive 3-D Cultivated Cell Imaging," *IEEE Sensors Journal,* vol. 18, no. 13, pp. 5402-5412, 2018.

[22] X. H. Hu and W. Q. Yang, "Planar capacitive sensors - designs and applications," (in English), *Sensor Review,* vol. 30, no. 1, pp. 24-39, 2010.

[23] Y. Yang, J. Jia, N. Polydorides, and H. McCann, "Effect of structured packing on EIT image reconstruction," in *Imaging Systems and Techniques (IST), 2014 IEEE International Conference on*, 2014, pp. 53-58: IEEE.

[24] M. Schmidt, G. Fung, and R. Rosales, "Fast optimization methods for L1 regularization: A comparative study and two new approaches," (in English), *Machine Learning: Ecml 2007, Proceedings,* vol. 4701, pp. 286-+, 2007.

[25] A. Wachter and L. T. Biegler, "Line search filter methods for nonlinear programming: Motivation and global convergence," (in English), *Siam Journal on Optimization,* vol. 16, no. 1, pp. 1-31, 2005.

[26] Y. J. Yang and J. B. Jia, "A multi-frequency electrical impedance tomography system for real-time 2D and 3D imaging," (in English), *Review of Scientific Instruments,* vol. 88, no. 8, Aug 2017.

[27] N. Polydorides, "Linearization Error in Electrical Impedance Tomography," (in English), *Progress in Electromagnetics Research-Pier,* vol. 93, pp. 323-337, 2009.

[28] B. Gong, B. Schullcke, S. Krüger-Ziolek, and K. Möller, "An Investigation of Modeling Error of EIT Reconstruction," *Journal of Biomedical Science and Engineering,* vol. 10, no. 05, p. 59, 2017.

[29] P. C. Hansen and D. P. O'Leary, "The use of the L-curve in the regularization of discrete ill-posed problems," *SIAM Journal on Scientific Computing,* vol. 14, no. 6, pp. 1487-1503, 1993.

[30] M. Belge, M. E. Kilmer, and E. L. Miller, "Efficient determination of multiple regularization parameters in a generalized L-curve framework," *Inverse Problems,* vol. 18, no. 4, p. 1161, 2002.

[31] J. Feng and N. Simon, "Gradient-based Regularization Parameter Selection for Problems with Non-smooth Penalty Functions," *Journal of Computational and Graphical Statistics,* no. just-accepted, 2017.

Yunjie Yang (M'13) received his B.Eng., M.Sc. and Ph.D. degrees from Anhui University, China, in 2010, Tsinghua University, China, in 2013, and The University of Edinburgh, UK, in 2018, respectively. After his Ph.D., he briefly worked as a Postdoctoral Research Associate in Chemical Species Tomography at The University of Edinburgh. Since September 2018, he has become a Chancellor's Fellow in Data Driven Innovation at School of Engineering, The University of Edinburgh. His research interests are in the areas of sensing and imaging with miscellaneous tomography modalities, and machine learning techniques for process analysis. He is the Associate Editor of IEEE Access and was the recipient of the 2015 IEEE I&M Society Graduate Fellowship Award.

Hancong Wu (S'16) received his BEng (Hons) degree both in Electronics and Electrical Engineering at the University of Edinburgh and in Electronic and Information Engineering at South China University of Technology in 2015. He is currently a PhD student with the Agile Tomography Group, University of Edinburgh. His research interests include biosensor design, impedance sensing, electrical impedance tomography and machine learning techniques for process analysis.

Jiabin Jia (M'15) received the Ph.D. degree from the University of Leeds, Leeds, U.K., in 2010, supported by the Overseas Research Students Award Scheme. He was a Research Fellow with the University of Leeds, where he was involved in the EPSRC Project, for three years. In 2013, he joined The University of Edinburgh, Edinburgh, U.K., where he is currently a Lecturer of electronic engineering, specializing in agile tomography research, with the School of Engineering, Institute for Digital Communications. He has authored or co-authored over 30 peer-reviewed journal publications and has contributed to and led a range of research projects funded by from different funding councils. His current research interests include electrical tomography, acoustic tomography, medical imaging, industrial process multiphase flow dynamics, real-time monitoring, and innovative diagnostic sensing for medical and industrial applications.

Pierre-Olivier Bagnaninchi is a principal investigator at the College of Medicine and Veterinary Medicine, at the University of Edinburgh, affiliated to the MRC Centre for Regenerative Medicine. Pierre-Olivier studied theoretical physics (MSc, 97) before moving to the field of biomedical engineering. He obtained his PhD in biomedical engineering in 2001 from the University of Grenoble, France in partnership with Thales. He then accepted a two-year post-doctoral position at McGill University in Prof. Maryam Tabrizian lab to develop impedance-based biosensors for tissue engineering applications. Following a PDRA in optical coherence tomography in 2004 at Keele University, he was awarded in 2008 a 5-year RCUK fellowship at the University of Edinburgh. He was then appointed principal investigator in 2013. His main research interest is the development of label-free quantitative monitoring technologies to monitor cell proliferation and differentiation in 2D and 3D cell cultures (organoids, gels and scaffolds).